



The selective hydrogenation of ethyl stearate to stearyl alcohol over Cu/Fe bimetallic catalysts



Limin He^{a,b,c}, Xiaoru Li^{a,b,c}, Weiwei Lin^{a,b,c}, Wei Li^{a,b,c}, Haiyang Cheng^{a,b}, Yancun Yu^{a,b}, Shin-ichiro Fujita^d, Masahiko Arai^d, Fengyu Zhao^{a,b,*}

^a State Key Laboratory of Electroanalytical Chemistry, Changchun Institute of Applied Chemistry, Chinese Academy of Sciences, Changchun 130022, PR China

^b Laboratory of Green Chemistry and Process, Changchun Institute of Applied Chemistry, Chinese Academy of Sciences, Changchun 130022, PR China

^c University of Chinese Academy of Sciences, Beijing 100049, PR China

^d Division of Chemical Process Engineering, Faculty of Engineering, Hokkaido University, Sapporo 060-8628, Japan

ARTICLE INFO

Article history:

Received 8 December 2013

Received in revised form 12 May 2014

Accepted 13 May 2014

Available online 23 May 2014

Keywords:

Cu/Fe catalyst

Synergistic effect

Hydrogenation

Ethyl stearate

ABSTRACT

Bimetallic and monometallic catalysts including Cu and/or Fe species were prepared by a co-precipitation method and their catalytic performance was tested for the selective hydrogenation of ethyl stearate to stearyl alcohol. The bimetallic catalysts were observed to be even more active for this selective hydrogenation compared to the monometallic catalysts and their physical mixtures. With a bimetallic catalyst of Cu/Fe (4/1 in mole ratio) reduced at 200 °C, a selectivity to the alcohol reached to above 99% at a conversion of 97% in reaction for 4 h at 230 °C, 3.0 MPa. Effects of composition and reduction temperature on the catalytic performance were studied and the properties of catalysts prepared under different conditions were examined by XRD, TPR, N₂ physisorption, and SEM. The relationship of the performance with the properties of the catalysts was discussed, along with the conditions under which synergistic effects of Cu and Fe species appeared and caused the enhancement of the catalytic performance.

© 2014 Elsevier B.V. All rights reserved.

1. Introduction

Fatty alcohols and their derivatives, especially higher alcohols, are industrially important intermediates in the synthesis of surfactants and plasticizers [1,2]. Higher alcohols are long chain fatty alcohols with a carbon number of 12–22, such as lauryl alcohol, cetyl alcohol and stearyl alcohol. The most commonly used method to produce fatty alcohols is the selective hydrogenation of fatty acids or fatty acid esters over heterogeneous catalysts [3,4]. Copper catalyst is a good candidate for the selective hydrogenation of C=O bond to alcohol without further hydrogenolysis of C—O bond formed [5,6]. Considering that copper itself is low active for this reaction, one should use supports or promoters to improve the activity and selectivity. Currently, copper catalysts, such as Cu/SiO₂, Cu/ZnO, Cu-Zn/Al₂O₃, have been widely studied for the selective hydrogenation of fatty esters to corresponding alcohols [7–9]. The influence of dispersion of Cu particles and the

activation of hydrogen molecule and fatty esters are of importance [10–12]. Recently, it was reported that iron could act as an electronic/chemical promoter to modify metal catalysts and improve their catalytic activity and selectivity because it increased surface area and dispersion of host metal elements [13–15]. For example, the electronegative metal of Fe could enhance the selectivity of hydrogenation of unsaturated aldehydes to unsaturated alcohols over Pt catalyst [16,17]. An Fe modified CoB amorphous alloy catalyst increased the selectivity to crotyl alcohol during the selective hydrogenation of crotonaldehyde [18]. Therefore, the Fe modified catalysts may produce preferential adsorption sites for the C=O bond, thus enhancing the selective hydrogenation of C=O to C—OH. This would be due to the changes in structural and/or electronic properties of Cu species caused by the addition of Fe.

In this work, we prepared two kinds of Cu/Fe bimetallic catalysts by co-precipitation method and their catalytic performances were discussed for the hydrogenation of ethyl stearate to stearyl alcohol as a model reaction. The composition of Cu/Fe catalysts was found to greatly influence their catalytic behavior. The correlation of their catalytic performance with the properties of Cu/Fe catalysts, such as phase composition, morphology, specific surface area, pore diameter, and pore volume was discussed in detail. Strong electronic interactions of Cu and Cu₂O with Fe₃O₄ and Lewis acid sites should play crucial roles for high yield of fatty alcohol

* Corresponding author at: State Key Laboratory of Electroanalytical Chemistry, Changchun Institute of Applied Chemistry, Chinese Academy of Sciences, Changchun 130022, PR China. Tel.: +86 431 85262 410; fax: +86 431 85262410.

E-mail address: zhaofy@ciac.ac.cn (F. Zhao).

observed in the selective hydrogenation of ethyl stearate to stearyl alcohol.

2. Experimental

2.1. Synthesis and characterization of catalysts

All chemicals used in the present work are analytical grade and used without further purification. The Cu/Fe catalysts were prepared by a simple co-precipitation method. Typically, an aqueous solution of cupric nitrate ($\text{Cu}(\text{NO}_3)_2 \cdot 3\text{H}_2\text{O}$, 0.25 M) was mixed with an aqueous solution of ferric nitrate ($\text{Fe}(\text{NO}_3)_3 \cdot 9\text{H}_2\text{O}$, 0.25 M) with a Cu/Fe molar ratio of either 1/4 or 4/1. After the mixture solution was stirred at 80 °C for 30 min, an aqueous solution of sodium hydroxide (NaOH, 1 M) was added dropwise to the salt solution under vigorously stirring until the pH reached to ca. 9–10. The mixture obtained was further stirred at 80 °C for 4 h and then aged for another 1 h at room temperature. The precipitate formed was filtrated, washed with distilled water for several times to remove the impurities, and then dried at 110 °C. The samples so prepared will be denoted as Cu/4Fe-pre and 4Cu/Fe-pre in which Cu/Fe ratio is 1/4 and 4/1, respectively. These samples were calcined at 300 °C for 4 h in air; the samples will be denoted as Cu/4Fe-C300 and 4Cu/Fe-C300, respectively. For comparison, monometallic oxide materials were also prepared by similar procedures. The samples prepared before and after the calcination will be denoted as Cu-pre (Fe-pre) and Cu-C300 (Fe-C300), respectively. The samples were further reduced in hydrogen atmosphere at different temperatures (150, 200 and 500 °C) for 90 min, which will be denoted, for example, as Cu/4Fe-R150.

The structure and crystal phase composition of the samples were determined by powder X-ray diffraction patterns with a Brucker D8 GADDS diffractometer using Co K radiation (1.79 Å) and the crystallite size was calculated with the Scherrer's equation. The samples for XRD examination were reduced at a certain temperature and reserved in ethanol for avoiding exposure to air before XRD tests. The temperature-programmed reduction (TPR) analysis was performed under a flow of 5% H_2/N_2 mixture (30 ml/min), with a heating rate of 10 K/min. Surface acidity was studied by NH_3 temperature-programmed desorption (TPD) on a TP-5080 Multi-functional Automatic Adsorption Instrument (Tianjin Xianquan Industry and Trade Development Co. Ltd, China) equipped with a TCD. Prior to the TPD experiments, 100 mg of the catalyst sample was pre-reduced in situ at 200 °C for 90 min in a N_2/H_2 gaseous mixture. The morphology of the samples was recorded by scanning electron microscope (SEM Hitachi S-4800). N_2 adsorption/desorption isotherms were measured using a Micromeritics ASAP 2020 Analyzer (USA). The surface areas were calculated using the Brunauer–Emmett–Teller (BET) equation. Pore volume (V_p) was estimated using the adsorption branch of the N_2 isotherm curve. Pore size distribution curves were calculated by the Barrett–Joyner–Halenda (BJH) method using adsorption branch of the N_2 isotherms.

2.2. Activity test

Reaction experiments were carried out in a 50 ml stainless steel autoclave. All the catalysts were pre-reduced in hydrogen at temperature (150, 200, 500 °C) for 90 min before the reaction. After reduction, the catalyst was transferred into the autoclave, in which 5.0 ml hexane was added as solvent, under the protection of hydrogen. After that, a certain amount of ethyl stearate was added and the autoclave was sealed. The reaction was operated under a stirring rate of 1300 rpm (without diffusion limitation) at 230 °C and a H_2 pressure of 3.0 MPa H_2 . After the reaction for several hours, the

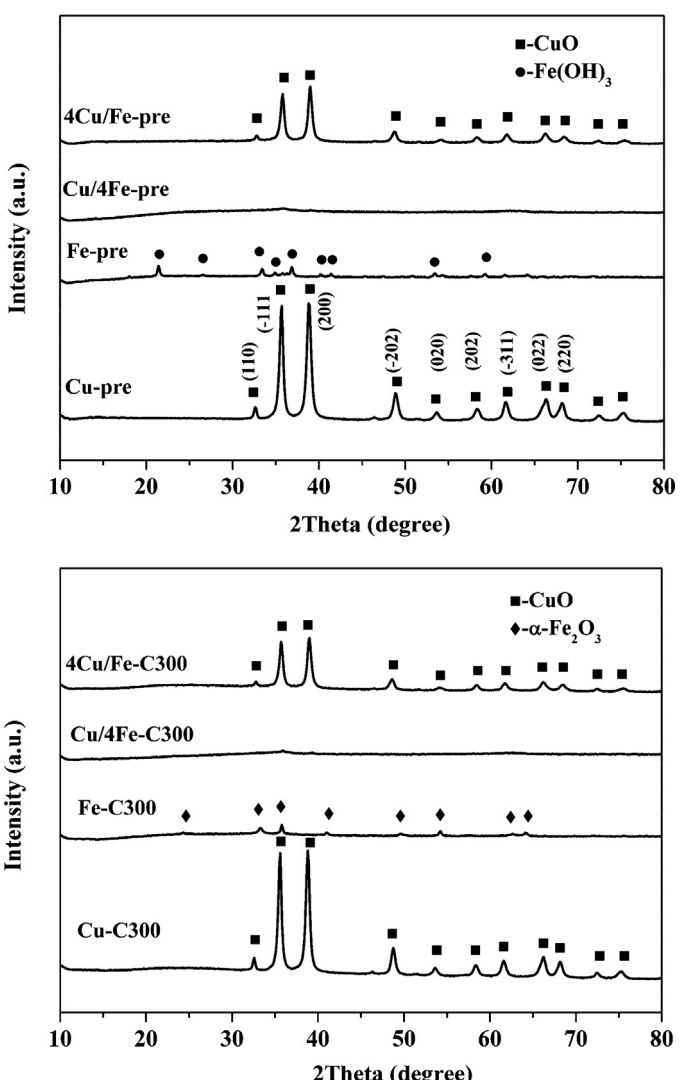


Fig. 1. XRD patterns of precursor and calcined samples.

autoclave was cooled to room temperature. The products were collected and then analyzed by gas chromatography with FID detector with a DB-1 capillary column and GC–MS.

3. Results and discussion

3.1. Textural properties and surface acidity

Fig. 1 shows the XRD patterns of the precursor and calcined Cu/Fe catalysts. The monometallic oxides, iron and copper oxides, were also analyzed for comparison. The Fe-pre sample gave a relative weak characteristic diffraction of $\text{Fe}(\text{OH})_3$ (JSCPDs 29-0713), and after calcination at 300 °C it was transferred to $\alpha\text{-Fe}_2\text{O}_3$ (JCPDS 33-0664). Both Cu-pre and Cu-C300 sample presented CuO phase. This is because that copper hydroxide $\text{Cu}(\text{OH})_2$ was metastable and thermodynamically easy to transfer into more stable compound of CuO [19]. In this system, the aging temperature was 80 °C so that the precipitate $\text{Cu}(\text{OH})_2$ formed was directly decomposed to CuO in the hot alkali solution [20]. For Cu/4Fe samples, no any diffraction peaks could be detected before and after the calcination at 300 °C, indicating that both the Cu and Fe existed in an amorphous state. Zhang et al. reported that a certain amount of Cu could prevent the crystallization of $\alpha\text{-Fe}_2\text{O}_3$, and more importantly it could increase the temperature of phase transformation from $\text{Fe}(\text{OH})_x$

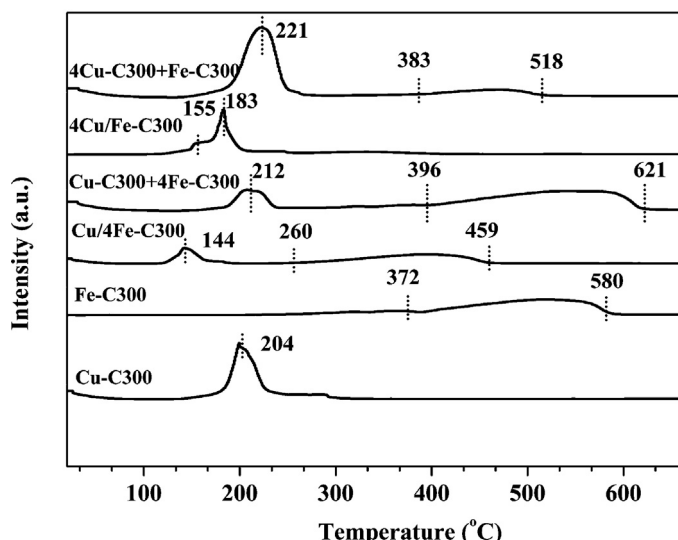


Fig. 2. TPR profiles of monometallic and bimetallic catalysts calcined at 300 °C. For comparison, physical mixtures of Cu-C300 + 4Fe-C300 and 4Cu-C300 + Fe-C300 (mixed in equal amounts).

to $\alpha\text{-Fe}_2\text{O}_3$ [21]. For 4Cu/Fe samples, strong diffraction peaks of CuO (JCPDS 48-1548) were observed, due to the high amount of Cu loaded. However, there was no any diffraction peak of iron species in precursor and calcined samples, indicating iron species existed in amorphous state in the 4Cu/Fe sample as well.

The hydrogen pre-reduction is a necessary and important process to activate the catalyst before its use. Fig. 2 shows the H_2 -TPR results of the calcined monometallic and bimetallic catalysts. A sharp and intensive reduction peak was observed for Cu-C300 at about 204 °C, which was assigned to the reduction of CuO to metallic Cu, but some Cu_2O species still remained in the sample reduced at 200 °C (Fig. 3). After reduction at 600 °C, CuO was almost reduced to metallic Cu with a very little amount of Cu_2O phase. For Fe-C300 sample, a weak peak at around 360 °C was assigned to the reduction of Fe_2O_3 to Fe_3O_4 , and a wide peak at around 518 °C (372–580 °C) to the further reduction of Fe_3O_4 to Fe. This reduction behavior is in accordance with the literature that the reduction of Fe_2O_3 occurs through two steps of Fe_2O_3 to Fe_3O_4 and then Fe_3O_4 to Fe [22]. Figs. 2 and 3 showed that Fe_2O_3 cannot be reduced at 200 °C but fully reduced to metallic Fe at 600 °C.

For comparison, physical mixtures of monometallic Cu and Fe samples were also examined, in which the Cu/Fe ratio was 1/4 or 4/1. The TPR patterns obtained were very similar to the sum of those monometallic samples. However, bimetallic Cu/Fe catalysts showed very different reduction behavior. The reduction peak of Cu/4Fe-C300 shifted to low temperature with a relatively broad peak at 144 °C compared to Cu-C300 sample. As for 4Cu/Fe catalyst, the reduction peak split into two peaks at low temperatures of 155 and 183 °C (Fig. 2). It is therefore suggested that there exist strong interactions between Cu and Fe species in the bimetallic catalysts.

The XRD patterns of bimetallic Cu/Fe catalysts reduced at different temperatures are shown in Fig. 4. For Cu/4Fe-R150 and Cu/4Fe-R200, only Fe_3O_4 (JCPDS 65-3107) was detected without any diffraction of copper species. As seen in Fig. 3, Fe_2O_3 cannot be reduced at 200 °C in the monometallic sample but it was reduced into Fe_3O_4 even at 150 °C in the bimetallic sample. These results indicated that the reduction temperature of Fe_2O_3 decreased in the presence of copper. After reduced at 500 °C, it showed characteristic diffraction peaks of metal Cu (JCPDS 04-0836) due to Cu (1 1 1) at 43.3°, Cu (2 0 0) at 50.4°, and Cu (2 2 0) at 74.1° and also metal Fe (JCPDS 06-0696) due to Fe (1 1 0) at 44.7°, Fe (0 0 4) at 65.0°, and Fe (2 1 1) at 82.3°.

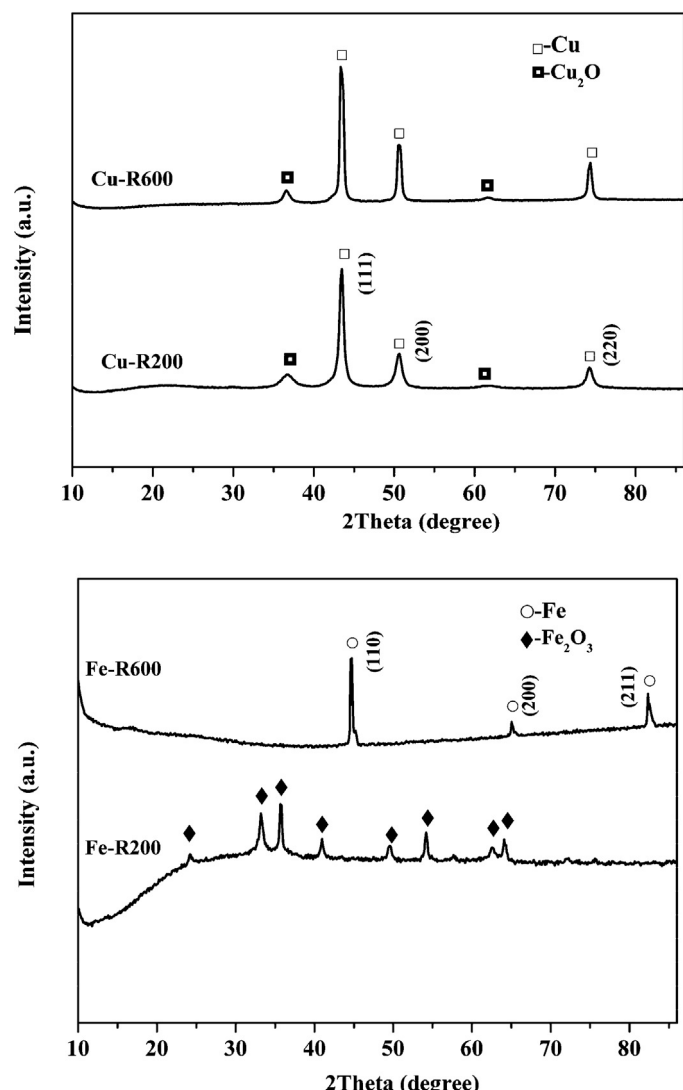


Fig. 3. XRD patterns of monometallic Cu and Fe samples after hydrogen reduction at 200 °C and 600 °C.

The 4Cu/Fe catalyst showed the diffraction peaks of Fe_3O_4 (JCPDS 65-3107) after reduced at 150 °C as shown in Fig. 4. The main metallic Cu (1 1 1) diffraction peak appears at 43.3° that is close to Fe_3O_4 (400) at 43.1°, so it is difficult to discriminate these two species. However, one can see clear metallic Cu (2 0 0) and Cu (2 2 0) crystal plane diffraction peaks at 50.4° and 74.1°. Therefore, Fe_3O_4 and Cu should co-exist in this sample. In addition, after reduced at 150 °C, the 4Cu/Fe catalyst still exhibited the characteristic diffraction peaks of CuO phase at 35.6° and 38.8° (JCPDS 65-2309). The diffraction peaks of CuO disappeared after it was reduced at 200 °C and the intensity of the diffraction peaks of Cu_2O (JCPDS 65-3288) at 36.5° and the metallic Cu (JCPDS 04-0836) at 43.3 °C increased when the reduction temperature increased from 150 °C to 200 °C. These results suggested that CuO species were gradually reduced to Cu_2O and Cu with increasing reduction temperature. After reduced at 200 °C, the 4Cu/Fe catalyst presented three kinds of species, Cu_2O , Cu and Fe_3O_4 . At high reduction temperature of 500 °C, it showed the strong diffraction peaks characteristic of metallic Cu (JCPDS 04-0836) and Fe (JCPDS 06-0696), indicating the complete reduction of CuO and Fe_2O_3 to their metallic states.

The SEM images of Cu/Fe catalysts collected before and after H_2 reduction at 150, 200, 500 °C are shown in Figure S1 (in the supporting information). The two kinds of the bimetallic

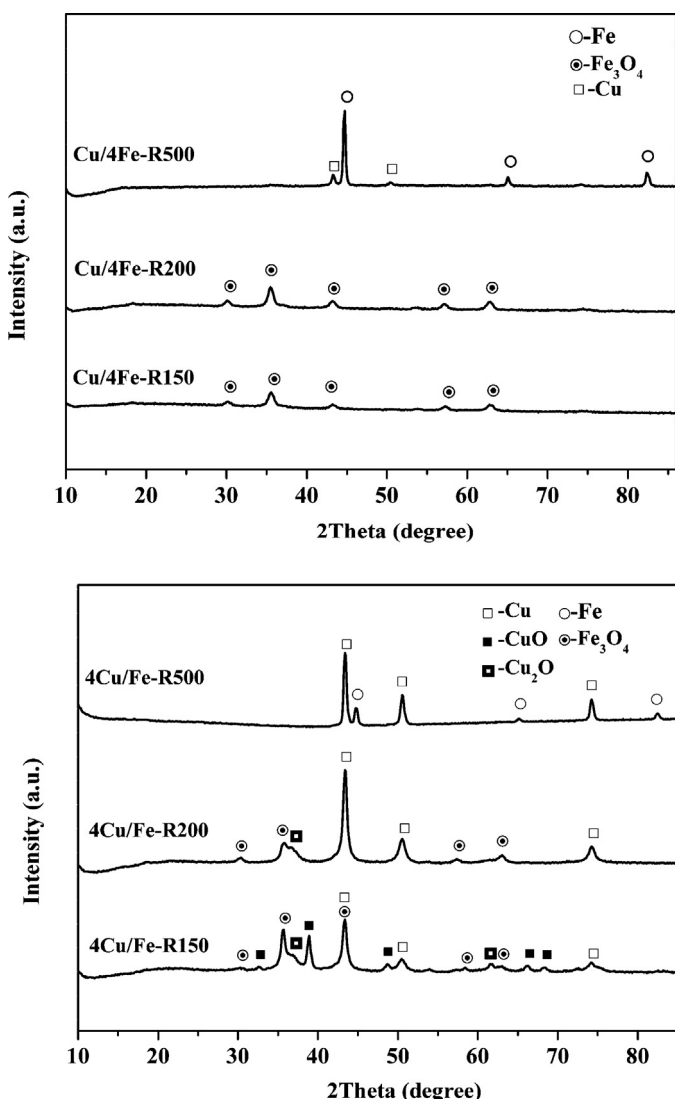


Fig. 4. XRD patterns of bimetallic Cu/Fe catalysts after reduction at different temperatures of 150 °C, 200 °C, and 500 °C.

catalysts different in the composition showed different morphologies. Before reduction, the Cu/4Fe catalyst showed spherical particles of ca. 60–100 nm in diameter but the 4Cu/Fe catalyst gave a shuttle or nanoplate structure of about 100 nm. After reduced at 150 °C and 200 °C, the spheres and nanoplates were assembled to big microspheres for both Cu/4Fe and 4Cu/Fe catalysts. Although exceptionally large particles were observed, most of the particles were well dispersed with particle size less than 120 nm. When the catalysts were reduced at a higher temperature of 500 °C, the particles aggregated significantly for Cu/4Fe catalyst as seen in Figure S1(d), while 4Cu/Fe catalyst showed a bright metal surface in Figure S1(h).

The Cu/Fe catalysts were further characterized by N₂ isotherms. The surface areas and pore size distributions are shown in Table 1 and Figure S2. The BET surface areas of unreduced Cu/Fe catalysts were extremely small, 4.8 m² g⁻¹ for Cu/4Fe catalyst and 7.9 m² g⁻¹ for 4Cu/Fe catalyst. After hydrogen reduction at 200 °C, the surface area of Cu/Fe catalysts considerably increased to 227.2 m² g⁻¹ for the former catalyst and 127.5 m² g⁻¹ for the latter. In addition, the pore volume slightly increased after hydrogen. The Cu/Fe catalysts are in micro- and mesoporous structures, which include mainly pores in the range of 2–9.5 nm as shown in Figure S2. The pore size distribution was rather wide for Cu/4Fe and 4Cu/Fe catalysts

Table 1
Surface areas and pore parameters of the calcined and reduced catalysts.

Catalyst	S _{BET} (m ² g ⁻¹)	V _p (cm ³ g ⁻¹)	D _p (nm)
Cu/4Fe-C300	4.8	0.16	3.76
Cu/4Fe-R200	227.2	0.34	3.75
4Cu/Fe-C300	7.9	0.31	9.46
4Cu/Fe-R200	127.5	0.43	3.42

The surface areas were calculated using the BET equation. Pore volume (V_p) was estimated using the adsorption branch of the N₂ isotherm curve. Average pore diameter (D_p) was estimated from BJH desorption determination.

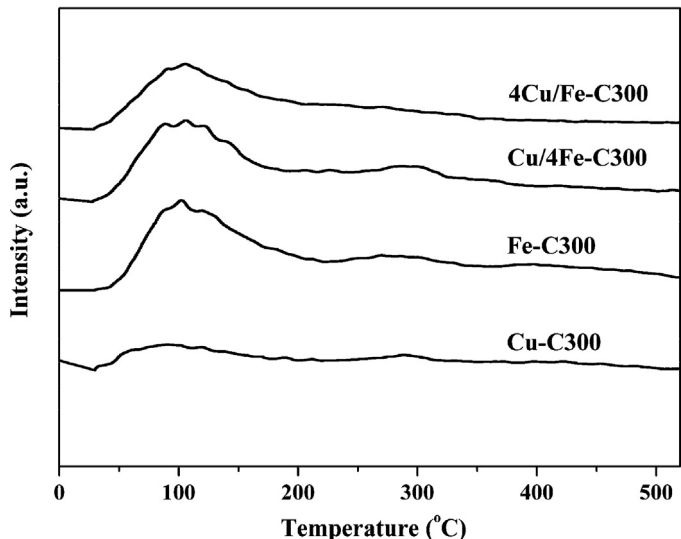


Fig. 5. NH₃-TPD profiles of monometallic and bimetallic samples.

before hydrogen reduction. After Cu/Fe catalysts were reduced at 200 °C, the larger pores of 9.5 nm and 7.6 nm disappeared and these showed narrow pore size distributions in the range of 2–6.4 nm. That is, the hydrogen reduction largely altered the morphology, surface area, pore size and pore volume of the Cu/Fe catalysts.

The distribution and strength of acidic sites of Cu/Fe catalysts were studied by NH₃-TPD. Before the NH₃-TPD tests, all the samples were pre-reduced in hydrogen at 200 °C for 90 min. Fig. 5 shows the NH₃ desorption patterns obtained. For CuO sample (Cu-C300, prepared in our experiment), a single weak desorption peak appeared at about 100 °C. CuO, as a common p-type semiconductor, typically has little Lewis acidic sites. The bimetallic Cu/4Fe and 4Cu/Fe catalysts possessed a broadly distributed desorption peaks around 100 °C which was similar to Fe-C300 sample. Lewis acid sites favor the activation of C=O through interactions with the electron pair of oxygen atom, which should result in the enhancement of the reactivity of carbonyl compounds, ethyl stearate in the present work. It was reported that Lewis acid sites of Cu/SiO₂ catalyst facilitated the conversion of dimethyl oxalate to ethanol [23].

3.2. Catalytic performance

The catalytic performance of monometallic and bimetallic samples was tested for the selective hydrogenation of ethyl stearate to stearyl alcohol (Scheme 1). The reaction results obtained are given in Tables 2 and 3. The present bimetallic Cu/Fe catalysts are very active and selective to the formation of stearyl



Scheme 1. Selective hydrogenation of ethyl stearate to stearyl alcohol.

Table 2

Catalytic performance of Cu/Fe catalysts in ester hydrogenation.

Entry	Catalyst	Conv. (%)	Select. (%)
1	CuO	5.0	98.5
2	Fe ₂ O ₃	–	–
3	Cu-C300 + 4Fe-C300	3.8	98.6
4	4Cu-C300 + Fe-C300	10.0	99.0
5	Cu/4Fe-C300	70.0	99.2
6	4Cu/Fe-C300	97.3	99.4

Reaction conditions: ethyl stearate 0.5 mmol, hexane 5.0 ml, catalyst 50 mg, H₂ 3.0 MPa, 230 °C, 4 h. All the catalysts were reduced in hydrogen at 200 °C for 90 min before reaction.

alcohol (entries 5,6), in which the selectivity to stearyl alcohol was above 99%. The monometallic catalyst and the physical mixtures of monometallic catalysts were also selective to the alcohol but even less active, the conversion being <10.0% (entries 1, 3, 4) as compared to 70.0% and 97.3% obtained with the bimetallic catalysts. The monometallic Fe sample has no activity, indicating that Cu species was the main active center during the selective hydrogenation of ethyl stearate to stearyl alcohol. These above results suggested the existence of interactions between Cu and Fe species in the Cu/Fe catalysts.

The influence of reduction temperature was examined for the two bimetallic catalysts. The reduction temperature had a significant effect on the catalytic activity as shown in **Table 3**. When the reduction temperature was raised from 150 °C to 200 °C, the catalytic activity increased for both Cu/4Fe and 4Cu/Fe catalysts. The conversion increased with the reaction time while keeping the high selectivity to stearyl alcohol. In addition, the 4Cu/Fe catalyst is more active than the Cu/4Fe. For example, when the catalysts were reduced at 150 °C, the conversion values of Cu/4Fe and 4Cu/Fe catalysts were 68.0% and 98.5% in 6 h, respectively. However, when Cu/Fe catalysts were reduced at a high temperature of 500 °C, the activity decreased sharply and the 4Cu/Fe became less active than Cu/4Fe. Which could be explained by (1) the seriously aggregation of the metal particles at high activation temperatures; (2) the Cu₂O disappeared at high reduction temperature, thus its function as the Lewis acid sites to accelerate the activation of C=O lost [24]; and (3) the Cu/4Fe with higher Fe content possesses more Lewis acid sites than 4Cu/Fe according to the results of NH₃-TPD in **Fig. 5**. In summary, the reduction temperature has strong influence on the activity of the Cu/Fe bimetallic catalysts, the 4Cu/Fe is more active than Cu/4Fe at the lower reduction temperature, while it is reverse at the higher reaction temperature due to the disappearance of advantages like the amount of active sites, Lewis acid sites

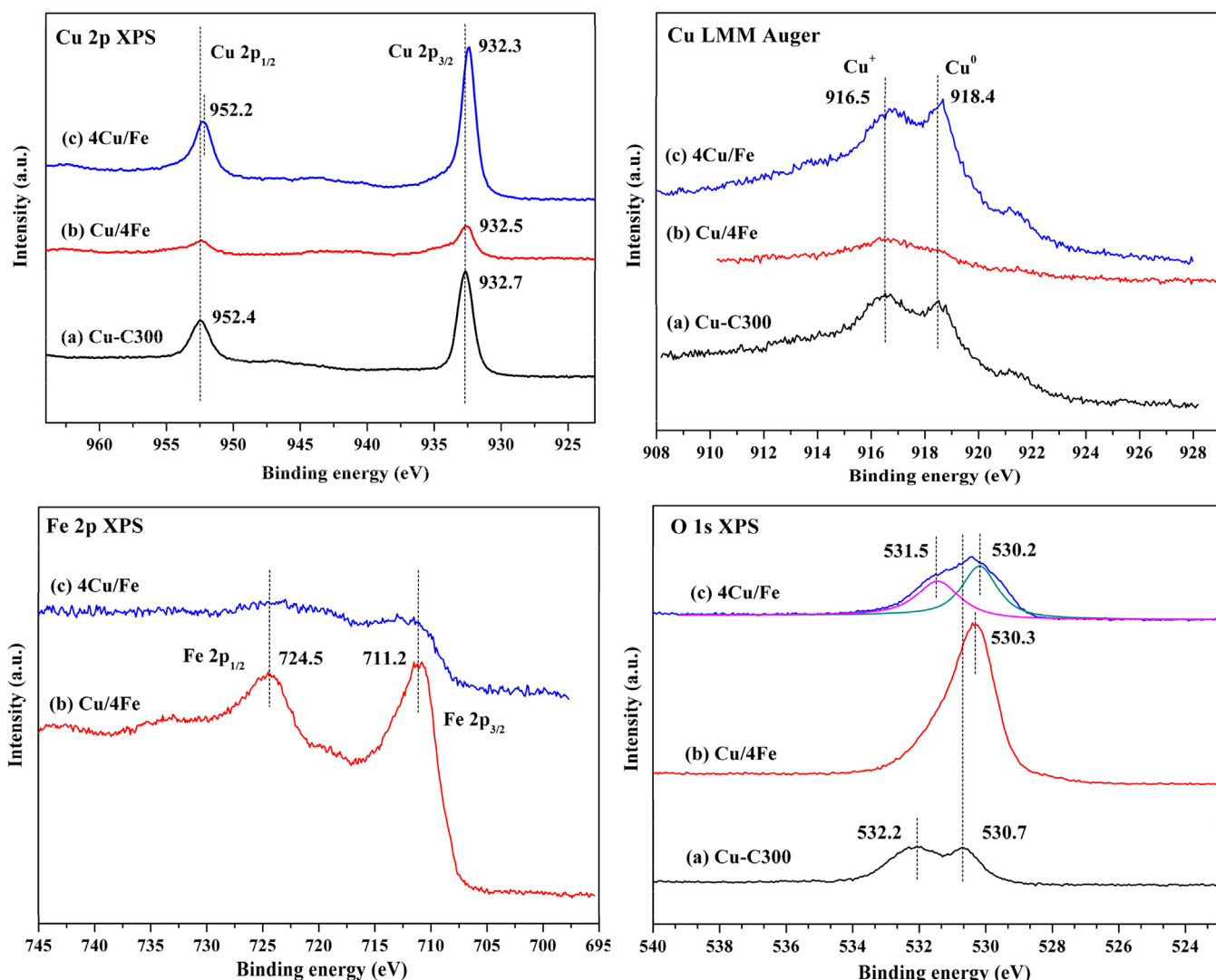


Fig. 6. XPS spectra of Cu 2p, Cu LMM, Fe 2p and O 1s of (a) Cu-C300, (b) Cu/4Fe and (c) 4Cu/Fe reduced at 200 °C.

Table 3

Catalytic performances of Cu/Fe catalysts reduced at different temperatures.

Catalyst	T (°C)	t (h)	Conv. (%)	Select. (%)
Cu/4Fe	150	1	21.6	98.3
		3	33.2	98.6
		6	68.0	98.4
	200	1	27.8	98.7
		4	70.0	99.2
		6	92.2	99.0
	500	8	10.0	99.1
		12	28.0	98.9
	4Cu/Fe	1	30.0	98.5
		3	45.1	98.3
		6	98.5	98.2
		1	51.9	98.4
		3	78.5	98.7
		4	97.3	99.4
		6	6.5	98.8
		12	10.5	99.0

Reaction conditions: ethyl stearate 0.5 mmol, hexane 5.0 ml, catalyst 50 mg, H₂ 3.0 MPa, 230 °C. The catalysts were reduced at T (°C) for 90 min before reaction.

of Cu₂O for the 4Cu/Fe catalyst, but the Lewis acid sites of Fe species become dominant factor to accelerate the reactivity of C=O bond for the Cu/4Fe catalyst at the higher reduction temperature.

3.3. The catalyst structure and activity relationship

The present results show that monometallic CuO and Fe₂O₃ catalysts and their physical mixtures are less active; however, the bimetallic Cu/Fe catalysts indicate much higher performance in the activity and selectivity. These strongly suggests that interactions exist between Cu and Fe species in these bimetallic catalysts, which was also suggested by H₂-TPR results that the reducibility of Cu and Fe species changed as compared to the monometallic catalysts (as shown in Fig. 2).

Further evidence of interaction between Cu and Fe was obtained from Ex situ XPS measurements. The XPS spectra of pure CuO, Cu/4Fe and 4Cu/Fe samples are shown in Fig. 6. The XPS spectra of Cu 2p appeared at the binding energies around 932.2–932.7 eV (Cu 2p_{3/2}) and 952.4 eV (Cu 2p_{1/2}) was ascribed to Cu⁰ and Cu⁺ [24], respectively, it is clearly that the copper species were reduced to Cu⁺ and Cu⁰ for all the samples reduced at 200 °C. However, the peak of Cu 2p_{3/2} for Cu/Fe samples shifted to the lower binding energies (932.3 eV and 932.5 eV) compared with that (932.7 eV) of pure CuO. It confirmed that an electronic interaction existed between Cu and Fe in the Cu/Fe bimetallic catalysts with an electron transferring from Fe to Cu. Moreover, we have further analyzed the Cu LMM Auger signals of Cu⁺ and Cu⁰, the peak at 918.4 eV is attributed to metallic copper Cu⁰, and the peak at 916.5 eV is assigned to Cu⁺ [25,26]. In addition, a plasmon satellite structure was resolved at binding energy of 920–922 eV, it is clear that the Cu⁰/Cu⁺ value on the surface of 4Cu/Fe is higher than that of Cu/4Fe catalyst, and thus the former presented higher activity. For the Cu/4Fe and 4Cu/Fe samples, they presented similar Fe 2p spectra, Fe 2p_{3/2} at about 711.2 eV and Fe 2p_{1/2} at about 724.5 eV, suggesting the Fe species in Cu/4Fe and 4Cu/Fe samples existed mainly as magnetite Fe₃O₄ [27,28], which is also consistent with the XRD results (in Fig. 4). In addition, the signal intensity of Fe 2p in 4Cu/Fe is much weaker than that in Cu/4Fe due to the lower Fe content. As for pure CuO, the peak of O 1s at 530.7 eV was the characteristic location of O²⁻, and peak at 532.2 eV was the chemisorbed oxygen [29]. While, for 4Cu/Fe, the peak of O 1s was broadened, indicating the presence of multi-component copper species. It was divided into two peaks, one at 530.2 eV attributes to O atoms bond to metals (Fe and Cu), and another at 531.5 eV associates with chemisorbed oxygen. But for the Cu/4Fe, only a single peak presented at 530.3 eV,

it mainly corresponds to the oxygen species of Fe₃O₄ due to the high content Fe, indicating that the Cu species mainly existed as Cu⁰ on the surface of Cu/4Fe, in agreement with the analysis from Cu 2p. Thus, it concluded that Cu⁺, Cu⁰ and Fe₃O₄ were the main species on the surface of Cu/Fe catalysts reduced at 200 °C based on both the results of XPS and XRD, and a stronger electronic interaction existed between the Cu and Fe as confirmed by the shift of the binding energy of Cu 2p. More importantly, the activity of Cu/Fe catalysts is consistent with the nature of active species on their surfaces.

The synergistic effects of Cu⁰/Cu⁺ species and Fe₃O₄ should be responsible for the high catalytic performance of 4Cu/Fe catalyst in selective hydrogenation of ethyl stearate to stearyl alcohol.

4. Conclusions

The bimetallic Cu/Fe catalysts, prepared by a co-precipitation method, show even higher performance in the selective hydrogenation of ethyl stearyl to stearyl alcohol with respect to the reaction rate and the selectivity to the alcohol, as compared to the monometallic catalysts and their physical mixtures. The activity depends on the composition of the catalysts; 4Cu/Fe catalyst is more active than the Cu/4Fe one while the selectivity to the alcohol is almost the same between the two catalysts. With the former catalyst reduced at 200 °C, a conversion of >97% and a selectivity of >99% can be achieved within 4 h at a reaction temperature of 230 °C. The high performance of this catalyst may result from synergistic effects of Cu and Fe species, for which the presence of Cu₂O, Cu and Fe₃O₄ should be requisite. Large surface area and Lewis acid sites present on the bimetallic catalysts may also be important factors. The Lewis acid sites are effective for the activation of the carbonyl group of the substrate.

Acknowledgements

The authors gratefully acknowledge the financial supports from NSFC 21273222, the JSPS-NSFC Bilateral Research Program, and from Jilin Province, China 20100562.

Appendix A. Supplementary data

Supplementary data associated with this article can be found, in the online version, at <http://dx.doi.org/10.1016/j.molcata.2014.05.009>.

References

- [1] M.B.O. Andersson, J.W. King, L.G. Blomberg, Green Chem. 2 (2000) 230–234.
- [2] P. Yuan, Z.Y. Liu, W.Q. Zhang, H.J. Sun, S.C. Liu, Chin. J. Catal. 31 (2010) 769–775.
- [3] S. Taniguchi, T. Makino, H. Watanuki, Y. Kojima, M. Sano, T. Miyake, Appl. Catal. A: Gen. 397 (2011) 171–173.
- [4] T. Miyake, T. Makino, S. Taniguchi, H. Watanuki, T. Niki, S. Shimizu, Y. Kojima, M. Sano, Appl. Catal. A: Gen. 364 (2009) 108–112.
- [5] K.L. Deutsch, B.H. Shanks, J. Catal. 285 (2012) 235–241.
- [6] A.Y. Yin, X.Y. Guo, W.L. Dai, K.N. Fan, J. Phys. Chem. C 113 (2009) 11003–11013.
- [7] S.R. Wang, L.J. Zhu, Y.Y. Zhu, X.L. Ge, X.B. Li, Chin. Chem. Lett. 22 (2011) 362–365.
- [8] H. Huang, S.H. Wang, S.J. Wang, G.P. Cao, Catal. Lett. 134 (2010) 351–357.
- [9] L. He, H. Cheng, G. Liang, Y. Yu, F. Zhao, Appl. Catal. A: Gen. 452 (2013) 88–93.
- [10] M. Behrens, F. Stuht, I. Kasatkina, S. Kuhl, M. Havecker, F. Abild-Pedersen, S. Zander, F. Girsdsies, P. Kurr, B.L. Kniep, M. Tovar, R.W. Fischer, J.K. Norskov, R. Schlogl, Science 336 (2012) 893–897.
- [11] M.V. Twigg, M.S. Spencer, Appl. Catal. A: Gen. 212 (2001) 161–174.
- [12] Q. Yang, J. Zhang, L. Zhang, H.Y. Fu, X.L. Zheng, M.L. Yuan, H. Chen, R.X. Li, Catal. Commun. 40 (2013) 37–41.
- [13] C. Bolm, J. Legros, J. Le Pailh, L. Zani, Chem. Rev. 104 (2004) 6217–6254.
- [14] Z. Guo, C.M. Zhou, D.M. Shi, Y.F. Wang, X.L. Jia, J. Chang, A. Borgna, C. Wang, Y.H. Yang, Appl. Catal. A: Gen. 435 (2012) 131–140.
- [15] H.J. Sun, Y.J. Pan, H.B. Jiang, S.H. Li, Y.X. Zhang, S.C. Liu, Z.Y. Liu, Appl. Catal. A: Gen. 464 (2013) 1–9.
- [16] P. Beccat, J.C. Bertolini, Y. Gauthier, J. Massardier, P. Ruiz, J. Catal. 126 (1990) 451–456.

- [17] J.P. Stassi, P.D. Zgolycz, S.R. de Miguel, O.A. Scelza, *J. Catal.* 306 (2013) 11–29.
- [18] Y. Pei, P.J. Guo, M.H. Qiao, H.X. Li, S.Q. Wei, H.Y. He, K. Fan, *J. Catal.* 248 (2007) 303–310.
- [19] Y. Cudennec, A. Lecerf, *Solid State Sci.* 5 (2003) 1471–1474.
- [20] Y.H. Ni, H. Li, L.A. Jin, J.M. Hong, *Cryst. Growth Des.* 9 (2009) 3868–3873.
- [21] B.T. Qiao, A.Q. Wang, J. Lin, L. Li, D.S. Su, T. Zhang, *Appl. Catal. B: Environ.* 105 (2011) 103–110.
- [22] G. Neri, A.M. Visco, S. Galvagno, A. Donato, M. Panzalorto, *Thermochim. Acta* 329 (1999) 39–46.
- [23] S. Zhao, H.R. Yue, Y.J. Zhao, B. Wang, Y.C. Geng, J. Lv, S.P. Wang, J.L. Gong, X.B. Ma, *J. Catal.* 297 (2013) 142–150.
- [24] L.F. Chen, P.J. Guo, M.H. Qiao, S.R. Yan, H.X. Li, W. Shen, H.L. Xu, K.N. Fan, *J. Catal.* 257 (2008) 172–180.
- [25] C.K. Wu, M. Yin, S. O'Brien, J.T. Koberstein, *Chem. Mater.* 18 (2006) 6054–6058.
- [26] S.Y. Zhang, G.L. Fan, F. Li, *Green. Chem.* 15 (2013) 2389–2393.
- [27] T. SchedelNiedrig, W. Weiss, R. Schlogl, *Phys. Rev. B* 52 (1995) 17449–17460.
- [28] R.F. Wang, J.C. Jia, H. Wang, Q.Z. Wang, S. Ji, Z.Q. Tian, *J. Solid State Electr.* 17 (2013) 1021–1028.
- [29] A.P. Grosvenor, B.A. Kobe, N.S. McIntyre, *Surf. Sci.* 572 (2004) 217–227.